Journal of Solid Mechanics Vol. 10, No. 1 (2018) pp. 1-22

Vibration Analysis of Magneto-Electro-Elastic Timoshenko Micro Beam Using Surface Stress Effect and Modified Strain Gradient Theory under Moving Nano-Particle

M. Mohammadimehr *, H. Mohammadi Hooyeh

Department of Solid Mechanics, Faculty of Mechanical Engineering, University of Kashan, Kashan, Iran

Received 1 September 2017; accepted 14 November 2017

ABSTRACT

In this article, the free vibration analysis of magneto-electro-elastic (MEE) Timoshenko micro beam model based on surface stress effect and modified strain gradient theory (MSGT) under moving nano-particle is presented. The governing equations of motion using Hamilton's principle are derived and these equations are solved using differential quadrature method (DQM). The effects of dimensionless electric potential, dimensionless magnetic parameter, material length scale parameter, external electric voltage, external magnetic parameter, slenderness ratio, temperature change, surface stress effect, two parameters of elastic foundation on the dimensionless natural frequency are investigated. It is shown that the effect of electric potential and magnetic parameter simultaneously increases the dimensionless natural frequency. On the other hands, with considering two parameters, the stiffness of MEE Timoshenko micro beam model increases. It can be seen that the dimensionless natural frequency of micro structure increases by MSGT more than modified couple stress theory (MCST) and classical theory (CT). It is found that by increasing the mass of nano-particle, the dimensionless natural frequency of system decreases. The results of this study can be employed to design and manufacture micro-devices to prevent resonance phenomenon or as a sensor to control the dynamic stability of micro structures.

Keywords: Vibration analysis; Moving nano-particle; Timoshenko micro beam model; Surface stress effect, MSGT; Magneto-electro-elastic loadings; DQM.

1 INTRODUCTION

MAGENTO-ELECTRO-ELASTIC (MEE) composite materials with piezoelectric and piezomagnetic phases can be utilized as materials providing energy conversion among magnetic, electric and mechanical energies [1]. These materials are applied in various applications such as structural health monitoring, vibration control, sensor and actuator applications, robotics, medical instruments and energy harvesting [2-5]. In recent years, static, buckling, and vibration analysis of MEE materials has found significance among many researchers. Bhangala and Ganesan [6] studied the free vibration of functionally graded (FG) non-homogeneous MEE cylindrical shell by using

*Corresponding author. Tel.: +98 31 5591 3432; Fax: +98 31 5591 2424.
E-mail address: mmohammadimehr@kashanu.ac.ir (M.Mohammadimehr).

the semi-analytical finite element approach. They illustrated that the piezoelectric effect has the tendency of stiffening the shell and hence increases the structural natural frequency but magnetic effect has a negative influence on the system frequency and reduces the natural frequency. Lang and Xuewu [7] analyzed the buckling and vibration analysis of FG magneto-electro-thermo-elastic circular cylindrical shells. Their result represented that influence of piezo-magnetic constant on the value of the critical thermal buckling load is more than that of piezoelectric constant.

Razavi and Shooshtari [8] investigated the nonlinear free vibration of MEE rectangular plates. In their work, it is observed that length-to-thickness ratio has negligible effect on the nonlinear frequency ratio in comparing with the effects of side ratio. Ke et al. [9] employed the free vibration of size-dependent MEE nanoplates based on the nonlocal elasticity theory. They obtained that the natural frequency is quite sensitive to the mechanical loading, electric loading and magnetic loading, while it is insensitive to the thermal loading. Li et al. [10] analyzed the buckling and free vibration of MEE nanoplate under Pasternak foundation based on Mindlin's plate theory. Their results depicted that the buckling load and vibration frequency decrease linearly with increasing of electric potential, spring and shear coefficients of the Pasternak foundation, and increases with an increase in the magnetic potential. Shooshtari and Razavi [11] studied linear and nonlinear free vibration of a multilayered MEE doubly-curved shell on elastic foundation. They showed that negative electric potentials and positive magnetic potentials increase the fundamental natural frequencies of MEE doubly curved shells, whereas the positive electric potentials and negative magnetic potentials have inverse effect on the natural frequency of MEE doubly-curved shells. They [12] also investigated large amplitude free vibration of symmetrically laminated MEE rectangular plates on Pasternak type foundation. Mohammadimehr et al. [13] investigated electro-elastic analysis of a sandwich thick plate considering FG core and composite piezoelectric layers on Pasternak foundation using third-order shear deformation theory (TSDT). Their results showed that the dimensionless natural frequency and critical buckling load decrease with increasing of the power law index, and vice versa for dimensionless deflection and electrical potential function, because of the sandwich thick plate with considering FG core becomes more flexible; while these results are reverse for thickness ratio. Ansari et al. [14] described nonlinear forced vibration of magneto-electro-thermo-elastic Nano beams based on Eringen's nonlocal elasticity theory. Their research showed that the effects of external magnetic potential and electric voltage are dependent on their sign. Xin and Hu [15] derived semi-analytical solutions for free vibration of arbitrary layered MEE beams using the state space approach (SSA) and discrete singular convolution (DSC) algorithm. Their results revealed that by increasing thickness natural frequency increases for higher mode and different material parameter affects natural frequency greatly. Also, they [16] obtained free vibration of multilayered MEE plates using SSA-DSC approach with simply supported boundary conditions. Based on strain gradient theory, Mohammadimehr et al. [17] investigated the free vibration analysis of tapered viscoelastic micro-rod resting on visco-Pasternak foundation. They assumed the material properties of micro-rod as the visco-elastic and modeled using the Kelvin-Voigt. Then, they derived the governing equation of motion of viscoelastic micro-rods using Hamilton's principle and energy method, and also solved these obtained equations using the differential quadrature method (DQM) for different boundary conditions. Their results showed that with an increase in the Winkler and Pasternak coefficients, the natural frequency increases as well as the obtained non-dimensional natural frequencies by modified couple stress theory (MCST) and strain gradient theory (SGT) decrease by increasing the material length to radius ratio. It was shown that the non-dimensional frequencies increase by increasing the damping coefficient for all theories. Moreover, at the specified value of damping coefficient of the elastic medium, the variation of non-dimensional natural frequency is approximately smooth. In the other work, Rahmati and Mohammadimehr [18] presented electro-thermo-mechanical vibration analysis of non-uniform and non-homogeneous boron nitride Nano rod (BNNR) embedded in elastic medium. They developed the steady state heat transfer equation without external heat source for non-homogeneous rod and derived temperature distribution. Also, using Maxwell′s equation and nonlocal elasticity theory, they obtained the coupled displacement and electrical potential equations and implemented the DQM to evaluate the natural frequencies. Ke and Wang [19] showed the free vibration of MEE Timoshenko Nano beams based on the nonlocal elasticity theory. They depicted that the natural frequency of nonlocal Nano beam is always smaller than that of the classical Nano beam, and it decreases with increasing of the nonlocal parameter. Wang et al. [20] analyzed axisymmetric bending of FG circular MEE plates of transversely isotropic materials based on linear three-dimensional elasticity theory. They represented that the electric potential and magnetic potential are parabolic-like along the thickness of the plate and this phenomenon may be considered in some approximate methods for bending of the MEE plates. Rao et al. [21] studied geometrically nonlinear finite rotation shell element for static analysis of layered MEE coupled composite structures. Mohammadimehr et al. [22] investigated free vibration of viscoelastic double-bonded polymeric nanocomposite plate reinforced by functionally graded-single walled carbon nanotubes (FG-SWCNTs) embedded in viscoelastic foundation based on modified strain gradient theory (MSGT). They defined material properties of

viscoelastic nanocomposite plates by extended mixture rule (EMR), and also extracted the governing equations of motion using Hamilton's principle and sinusoidal shear deformation theory. Then, they determined natural frequency of nanocomposite plates by Navier's and meshless methods, and also, using meshless method, the effect of various boundary conditions on dimensionless natural frequency. In the other work, they [23] extended modified strain gradient Reddy rectangular plate theory for biaxial buckling and bending analysis of double-coupled polymeric nanocomposite plates reinforced by functionally graded single-walled boron nitride nanotubes (FG-SWBNNTs) and FG-SWCNTs. Kattimani and Ray [24] investigated control of geometrically nonlinear vibrations of functionally graded MEE plates. Their results revealed that the electro-elastic and the magneto-elastic couplings have negligible influence on the nonlinear transient response of the FG MEE plates while increasing the stiffening effect marginally. Liu et al. [25] proposed guided wave propagation and mode differentiation in the layered MEE hollow cylinder. They illustrated that in a low frequency range, radius-thickness ratio have significant effect on the wave characteristics. Sedighi and Farjam [26] presented a modified model for dynamic instability of CNT based actuators by considering rippling deformation, tip-charge concentration and Casimir attraction. They concluded that the tip charge concentration and rippling phenomenon can substantially affect the electromechanical performance of actuators fabricated from cantilever CNT. Zare [27] considered pull-in instability behavior analysis of functionally graded micro-cantilevers under suddenly DC voltage. By employing modern asymptotic approach namely homotopy perturbation method with an auxiliary term, he obtained high-order frequency-amplitude relation, then the influences of material properties and actuation voltage on dynamic pull-in behavior are investigated. Sedighi [28] illustrated the influence of small scale on the pull-in behavior of nonlocal nano bridges considering surface effect, Casimir and van der Waals attractions. He investigated the effects of applied voltage and intermolecular parameters on pull-in instability as well as the natural frequency. Furthermore, he considered the influence of nonlocal parameter and surface energy on the dynamic pull-in voltage.

The effects of material length scale parameters on the rotation angle, dimensionless electric potential, and dimensionless magnetic parameter are taken into account. Also, the influences of dimensionless electric potential, dimensionless magnetic parameter, material length scale parameter, external electric voltage, external magnetic parameter, slenderness ratio, temperature change, surface stress effect, spring Winkler constant, and shear Pasternak constant on the dimensionless natural frequency are investigated.

2 THE GOVERNING EQUATIONS OF MOTION FOR MEE TIMOSHENKO MICRO BEAM MODEL

The governing equations of motion using Hamilton's principle are derived for magneto-electro-elastic (MEE) Timoshenko micro beam model based on surface stress effect and modified strain gradient theory (MSGT) under moving nano-particle and these equations are solved using differential quadrature method (DQM).

2.1 Modified strain gradient theory

The size dependent effect has an important role at micro scale. Fleck and Hutchinson [29-31] extended and reformulated the classical couple stress theory and renamed it as the strain gradient elasticity theory (SGET), in which for homogeneous isotropic and incompressible materials, three additional higher-order material length scale parameters are introduced. Lam et al. [32] proposed a modified strain gradient elasticity theory (MSGT) in which a new additional equilibrium equations to govern the behavior of higher-order stresses, the equilibrium of moments of couples is introduced, in addition to the classical equilibrium equations of forces and moments of forces. Meanwhile, there are only three independent higher-order materials length scale parameters for isotropic linear elastic materials in the present theory.

According to the modified strain gradient theory (MSGT) proposed by Lam et al. [32], the strain energy of a linear MEE continuum occupying region Ω is written as follows [22, 25, 33, and 34]:

$$U = \frac{1}{2}\int_{\Omega}(\sigma_{ij}\varepsilon_{ij} + p_i\gamma_i + \tau_{ijk}^{(1)}\eta_{ijk}^{(1)} + m_{ij}\chi_{ij} - \mathrm{D}_i\mathrm{E}_i - B_iH_i)dV \tag{1}$$

where $\varepsilon_{ij}, \gamma_i, \eta_{ijk}^{(1)}, \chi_{ij}, E_i, H_i$ denote the strain, the dilatation gradient tensor, the symmetric rotation gradient tensor, the deviatoric stretch gradient tensor, the electric field and magnetic field, respectively, which are defined by following form [10, 33, and 34]:

$$\varepsilon_{ij} = \frac{1}{2}(u_{i,j} + u_{j,i}) \tag{2}$$

$$\gamma_i = \varepsilon_{mm,i} \tag{3}$$

$$\eta_{ijk}^{(1)} = \frac{1}{3}(\varepsilon_{jk,i} + \varepsilon_{ki,j} + \varepsilon_{ij,k}) - \frac{1}{15}\delta_{ij}\left(\varepsilon_{mm,k} + 2\varepsilon_{mk,m}\right) - \frac{1}{15}\delta_{jk}\left(\varepsilon_{mm,i} + 2\varepsilon_{mi,m}\right) - \frac{1}{15}\delta_{ki}\left(\varepsilon_{mm,j} + 2\varepsilon_{mj,m}\right) \tag{4}$$

$$\chi_{ij} = \frac{1}{2}(\theta_{i,j} + \theta_{j,i}) \quad \theta_i = \frac{1}{2}(\text{curl(u)})_i \tag{5}$$

$$E_i = -\phi_{,i} \tag{6}$$

$$H_i = -\Gamma_{,i} \tag{7}$$

In which $u_i, \varepsilon_{mm}, \theta_i, \phi$ and Γ represent the displacement vector, dilatation strain, the infinitesimal rotation vector, electric and magnetic potentials respectively. δ_{ij} and e_{ijk} are the Knocker and the alternate symbols respectively. The basic equations for a MEE material may be expressed as follows:

$$\sigma_{ij} = c_{ijkl}\varepsilon_{kl} - e_{mij}E_m - q_{nij}H_n - \beta_{ij}\Delta T \tag{8}$$

$$D_i = e_{ikl}\varepsilon_{kl} + s_{im}E_m + d_{in}H_n + v_i\Delta T \tag{9}$$

$$B_i = q_{ikl}\varepsilon_{kl} + d_{im}E_m + \alpha_{in}H_n + \lambda_i\Delta T \tag{10}$$

In which $\sigma_{ij}, \varepsilon_{ij}, D_i, E_i, B_i$ and H_i are the stress, strain, electric displacement, electric field, magnetic induction and magnetic field, respectively. $c_{ijkl}, e_{mij}, q_{nij}, s_{im}, d_{in}, \alpha_{in}, v_i$ and λ_i are the elastic, piezoelectric, piezo-magnetic, dielectric constant, magneto-electric, magnetic, pyroelectric and pyro-magnetic constants, respectively. β_{ij} and ΔT are the thermal moduli and temperature change, respectively. The higher-order stresses $p_i, \tau_{ijk}^{(1)}$ and m_{ij} are given by [33, 34]:

$$p_i = 2\mu l_0^2 \gamma_i \tag{11}$$

$$\tau_{ijk}^{(1)} = 2\mu l_1^2 \eta_{ijk}^{(1)} \tag{12}$$

$$m_{ij} = 2\mu l_2^2 \chi_{ij} \tag{13}$$

where μ is the shear modulus and (l_0, l_1, l_2) are independent material length scale parameters.

2.2 Surface stress effect

The ratio of surface to volume at nano and micro structure is high, therefore the surface stress has important role and should be considered in analyze of these structures. The classical stress tensor related to the surface can be calculated using Gurtin and Murdoch theory [35-38]:

$$\sigma_{xx}^s = \tau_0^s + c_{11}^s\varepsilon_{xx}^s - e_{31}^s E_z - q_{31}^s H_z \tag{14}$$

where $\tau_0^s, c_{11}^s, \varepsilon_{xx}^s, e_{31}^s$ and q_{31}^s are the residual surface stress, elastic modulus, normal strain, piezoelectric and piezo magnetic constants in surface layer, respectively. The higher-order surface stresses $p_i^s, \tau_{ijk}^{(1)s}$ and m_{ij}^s can be expressed as [39]:

$$p_i^s = 2\mu_s l_0^2 \gamma_i^s \tag{15}$$

$$\tau_{ijk}^{(1)s} = 2\mu_s l_1^2 \eta_{ijk}^{(1)s} \tag{16}$$

$$m_{ij}^s = 2\mu_s l_2^2 \chi_{ij}^s \tag{17}$$

In which $\gamma_i^s, \eta_{ijk}^{(1)s}, \chi_{ij}^s$ and μ_s are the surface dilatation gradient tensor, the surface symmetric rotation gradient tensor, the surface deviatoric stretch gradient tensor and surface shear moduli, respectively.

2.3 MEE Timoshenko micro beam model

A schematic view of MEE micro-beam subjected to an electric and magnetic potentials and a uniform temperature with considering surface layer rand elastic medium under moving nano-particle is shown in Fig. 1. The displacement fields based on Timoshenko micro-beam model can be expressed as follows [40-41]:

$$\bar{u}_1(x, z, t) = u(x, t) - z\psi(x, t) \tag{18}$$

$$\bar{u}_2(x, z, t) = 0 \tag{19}$$

$$\bar{u}_3(x, z, t) = w(x, t) \tag{20}$$

where u and w are axial and transverse displacements for neutral axis, respectively, and ψ is the rotation angle of a transverse normal about the x-axis.

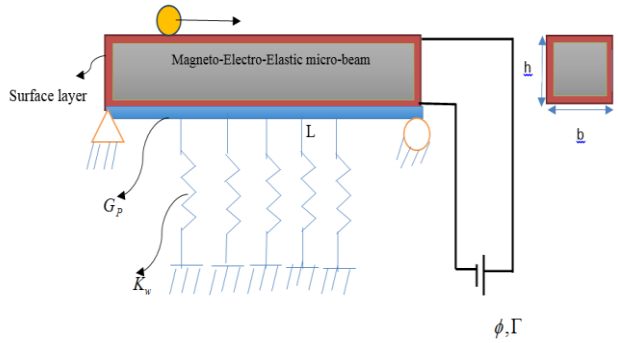

Fig.1
A schematic view of MEE micro-beam with considering surface layer and elastic medium under moving micro-particle.

The electric and magnetic potential distributions along the thickness direction of micro-beam are considered as follows [19], [42]:

$$\begin{aligned} \phi(x, z, t) &= -\cos(\beta z)\varphi_E(x, t) + \frac{2z V_E}{h} \\ \Gamma(x, z, t) &= -\cos(\beta z)\Upsilon_H(x, t) + \frac{2z \Omega_H}{h} \end{aligned} \tag{21}$$

where $\beta = \frac{\pi}{h}, \varphi_E(x,t)$ and $\Upsilon_H(x,t)$ are the variation of electric and magnetic potentials in the x -direction which must satisfy the electric and magnetic boundary conditions. V_E and Ω_H are the external electric voltage and external magnetic parameter, respectively.

By substituting Eqs. (18)- (20) into Eq. (2), the components of normal and shear strains for both bulk and surface are given by:

$$\varepsilon_{xx} = \varepsilon_{xx}^s = \frac{\partial u}{\partial x} - z\frac{\partial \psi}{\partial x} \tag{22}$$

$$\gamma_{xz} = \frac{\partial w}{\partial x} - \psi \ , \gamma_{xz}^s = 0 \tag{23}$$

Using Eqs. (3), (22), (23), the following equations are obtained:

$$\gamma_x = \gamma_x^s = \frac{\partial^2}{\partial x^2}u - z\frac{\partial^2}{\partial x^2}\psi \tag{24}$$

$$\gamma_z = \gamma_z^s = -\frac{\partial}{\partial x}\psi \tag{25}$$

By employing Eqs. (4), (22), (23), the non-zero component of deviatoric stretch gradient tensor yields:

$$\begin{aligned}
&\eta_{111}^{(1)} = \eta_{111}^{s(1)} = \frac{2}{5}\frac{\partial^2 u}{\partial x^2} - \frac{2}{5}z\frac{\partial^2 \psi}{\partial x^2} \\
&\eta_{333}^{(1)} = \frac{2}{5}\frac{\partial \psi}{\partial x} - \frac{1}{5}\frac{\partial^2 w}{\partial x^2} \ , \eta_{333}^{s(1)} = \frac{1}{5}\frac{\partial \psi}{\partial x} \\
&\eta_{113}^{(1)} = \eta_{131}^{(1)} = \eta_{311}^{(1)} = -\frac{8}{15}\frac{\partial \psi}{\partial x} + \frac{4}{15}\frac{\partial^2 w}{\partial x^2} \ , \eta_{113}^{s(1)} = \eta_{131}^{s(1)} = \eta_{311}^{s(1)} = -\frac{4}{15}\frac{\partial \psi}{\partial x} \\
&\eta_{313}^{(1)} = \eta_{331}^{(1)} = \eta_{133}^{(1)} = \eta_{313}^{s(1)} = \eta_{331}^{s(1)} = \eta_{133}^{s(1)} = -\frac{1}{5}\frac{\partial^2 u}{\partial x^2} + \frac{1}{5}z\frac{\partial^2 \psi}{\partial x^2} \\
&\eta_{122}^{(1)} = \eta_{212}^{(1)} = \eta_{221}^{(1)} = \eta_{122}^{s(1)} = \eta_{212}^{s(1)} = \eta_{221}^{s(1)} = -\frac{1}{5}\frac{\partial^2 u}{\partial x^2} + \frac{1}{5}z\frac{\partial^2 \psi}{\partial x^2} \\
&\eta_{322}^{(1)} = \eta_{232}^{(1)} = \eta_{223}^{(1)} = \frac{2}{15}\frac{\partial \psi}{\partial x} - \frac{1}{15}\frac{\partial^2 w}{\partial x^2} \ , \eta_{322}^{s(1)} = \eta_{232}^{s(1)} = \eta_{223}^{s(1)} = \frac{1}{15}\frac{\partial \psi}{\partial x}
\end{aligned} \tag{26}$$

By substituting Eqs. (22), (23) into Eq. (5) leads to the following equation:

$$\chi_{xy} = \chi_{yx} = \chi_{xy}^s = \chi_{yx}^s = -\frac{1}{4}\left(\frac{\partial^2 w}{\partial x^2} + \frac{\partial \psi}{\partial x}\right) \tag{27}$$

The higher-order stresses can be obtained by substituting Eqs. (24) - (27) into Eqs. (11)- (13) and (15)-(17) as follows:

$$
\begin{aligned}
&\tau_{111}^{(1)}=\tau_{111}^{(1)s}=\frac{4}{5}\mu l_1^2\frac{\partial^2 u_0}{\partial x^2}-\frac{4}{5}\mu l_1^2 z\frac{\partial^2\psi_0}{\partial x^2}\\
&\tau_{313}^{(1)}=\tau_{331}^{(1)}=\tau_{133}^{(1)}=\tau_{313}^{(1)s}=\tau_{331}^{(1)s}=\tau_{133}^{(1)s}=-\frac{2}{5}\mu l_1^2\frac{\partial^2 u_0}{\partial x^2}+\frac{2}{5}\mu l_1^2 z\frac{\partial^2\psi_0}{\partial x^2}\\
&\tau_{333}^{(1)}=\frac{4}{5}\mu l_1^2\frac{\partial\psi_0}{\partial x}-\frac{2}{5}\mu l_1^2\frac{\partial^2 w_0}{\partial x^2},\tau_{333}^{(1)s}=\frac{2}{5}\mu l_1^2\frac{\partial\psi_0}{\partial x}\\
&\tau_{113}^{(1)}=\tau_{131}^{(1)}=\tau_{311}^{(1)}=-\frac{16}{15}\mu l_1^2\frac{\partial\psi_0}{\partial x}+\frac{8}{15}\mu l_1^2\frac{\partial^2 w_0}{\partial x^2},\tau_{113}^{(1)s}=\tau_{131}^{(1)s}=\tau_{311}^{(1)s}=-\frac{8}{15}\mu l_1^2\frac{\partial\psi_0}{\partial x}\\
&\tau_{122}^{(1)}=\tau_{212}^{(1)}=\tau_{221}^{(1)}=\tau_{122}^{(1)s}=\tau_{212}^{(1)s}=\tau_{221}^{(1)s}=-\frac{2}{5}\mu l_1^2\frac{\partial^2 u_0}{\partial x^2}+\frac{2}{5}\mu l_1^2 z\frac{\partial^2\psi_0}{\partial x^2}\\
&\tau_{322}^{(1)}=\tau_{232}^{(1)}=\tau_{223}^{(1)}=\frac{4}{15}\mu l_1^2\frac{\partial\psi_0}{\partial x}-\frac{2}{15}\mu l_1^2\frac{\partial^2 w_0}{\partial x^2},\tau_{322}^{(1)s}=\tau_{232}^{(1)s}=\tau_{223}^{(1)s}=\frac{2}{15}\mu l_1^2\frac{\partial\psi_0}{\partial x}
\end{aligned}
\tag{28}
$$

$$
\begin{aligned}
&m_{xy}=m_{yx}=m_{xy}^s=m_{yx}^s=-\frac{1}{2}\mu l_2^2\left(\frac{\partial^2 w_0}{\partial x^2}+\frac{\partial\psi_0}{\partial x}\right)\\
&p_x=p_x^s=2\mu l_0^2\left(\frac{\partial^2 u_0}{\partial x^2}-z\frac{\partial^2\psi_0}{\partial x^2}\right)\\
&p_z=p_z^s=-2\mu l_0^2\frac{\partial\psi_0}{\partial x}
\end{aligned}
\tag{29}
$$

2.4 Plane stress state

If consider that micro-beam is under the plane stress state, the constitutive equations in one-dimensional form can be written as follows:

$$
\begin{aligned}
&\sigma_{xx}=\bar{c}_{11}\varepsilon_{xx}+\bar{e}_{31}(\beta\sin(\beta z)\varphi_E+\frac{2V_E}{h})+\bar{q}_{31}(\beta\sin(\beta z)\Upsilon_H+\frac{2\Omega_H}{h})-\bar{\beta}_1\Delta T\\
&\sigma_{xz}=\bar{c}_{44}\gamma_{xz}-\bar{e}_{15}\cos(\beta z)\frac{\partial\varphi_E}{\partial x}-\bar{q}_{15}\cos(\beta z)\frac{\partial\Upsilon_H}{\partial x}\\
&D_x=\bar{e}_{15}\gamma_{xz}+\bar{s}_{11}\cos(\beta z)\frac{\partial\varphi_E}{\partial x}+\bar{d}_{11}\cos(\beta z)\frac{\partial\Upsilon_H}{\partial x}\\
&D_z=\bar{e}_{31}\varepsilon_{xx}-\bar{s}_{33}(\beta\sin(\beta z)\varphi_E+\frac{2V_E}{h})-\bar{d}_{33}(\beta\sin(\beta z)\Upsilon_H+\frac{2\Omega_H}{h})+\bar{v}_3\Delta T\\
&B_x=\bar{q}_{15}\gamma_{xz}+\bar{d}_{11}\cos(\beta z)\frac{\partial\varphi_E}{\partial x}+\bar{\alpha}_{15}\cos(\beta z)\frac{\partial\Upsilon_H}{\partial x}\\
&B_z=\bar{q}_{31}\varepsilon_{xx}-\bar{d}_{33}(\beta\sin(\beta z)\varphi_E+\frac{2V_E}{h})-\bar{\alpha}_{33}(\beta\sin(\beta z)\Upsilon_H+\frac{2\Omega_H}{h})+\bar{\lambda}_3\Delta T
\end{aligned}
\tag{30}
$$

In which $\bar{c}_{ij},\bar{e}_{ij},\bar{q}_{ij},\bar{s}_{ij},\bar{\beta}_{ij},\bar{d}_{ij},\bar{\alpha}_{ij},\bar{v}_i$ and $\bar{\lambda}_i$ are elastic, piezoelectric, piezo-magnetic, dielectric constant, thermal moduli, magneto-electric, magnetic, pyroelectric and pyro-magnetic constants, respectively for MEE micro-beam under plane stress state. These constants are written in Appendix A with details.

The total strain energy with considering the strain gradient theory and the surface effect theory is written as follows:

$$
\begin{aligned}
&U^b+U^s=\frac{1}{2}\int_\Omega(\sigma_{ij}\varepsilon_{ij}+p_i\gamma_i+\tau_{ijk}^{(1)}\eta_{ijk}^{(1)}+m_{ij}\chi_{ij}-\mathrm{D}_i\mathrm{E}_i-B_iH_i)dA\,dx\\
&+\frac{1}{2}\int_\Omega(\sigma_{ij}^s\varepsilon_{ij}^s+p_i^s\gamma_i^s+\tau_{ijk}^{s(1)}\eta_{ijk}^{s(1)}+m_{ij}^s\chi_{ij}^s)dS dx
\end{aligned}
\tag{31}
$$

where U^b and U^s are the strain energy for the bulk and surface, respectively. By substituting Eqs. (6), (7), (11)-(13), (15)-(17) and (22)-(30) into Eq. (31), the total strain energy is obtained as follows:

$$\begin{aligned}
U^b+U^s &= \frac{1}{2}\int_0^L \{\left(\mathrm{N}+\tilde{\mathrm{N}}\right)\left(\frac{\partial u_0}{\partial x}\right)-\left(M+\tilde{M}\right)\left(\frac{\partial \psi_0}{\partial x}\right)+\left(Q\right)\left(\frac{\partial w_0}{\partial x}-\psi_0\right)+\left(P_1+\tilde{P}_1\right)\left(\frac{\partial^2 u_0}{\partial x^2}\right)\\
&-\left(P_3+\tilde{P}_3\right)\left(\frac{\partial \psi_0}{\partial x}\right)-\left(M_1^{(1)}+\tilde{M}_1^{(1)}\right)\left(\frac{\partial^2 \psi_0}{\partial x^2}\right)+\left(T_{111}^{(1)}+\tilde{T}_{111}^{(1)}\right)\left(\frac{2}{5}\frac{\partial^2 u_0}{\partial x^2}\right)\\
&-\left(M_{111}^{(1)}+\tilde{M}_{111}^{(1)}\right)\left(\frac{2}{5}\frac{\partial^2 \psi_0}{\partial x^2}\right)+\left(T_{333}^{(1)}\right)\left(\frac{2}{5}\frac{\partial \psi_0}{\partial x}-\frac{1}{5}\frac{\partial^2 w_0}{\partial x^2}\right)+\left(\tilde{T}_{333}^{(1)}\right)\left(\frac{1}{5}\frac{\partial \psi_0}{\partial x}\right)\\
&+3\left(T_{113}^{(1)}\right)\left(-\frac{8}{15}\frac{\partial \psi_0}{\partial x}+\frac{4}{15}\frac{\partial^2 w_0}{\partial x^2}\right)-3\left(\tilde{T}_{113}^{(1)}\right)\left(\frac{4}{15}\frac{\partial \psi_0}{\partial x}\right)+3\left(T_{223}^{(1)}\right)\left(\frac{2}{15}\frac{\partial \psi_0}{\partial x}-\frac{1}{15}\frac{\partial^2 w_0}{\partial x^2}\right)\\
&+3\left(\tilde{T}_{223}^{(1)}\right)\left(\frac{1}{15}\frac{\partial \psi_0}{\partial x}\right)+6\left(T_{221}^{(1)}+\tilde{T}_{221}^{(1)}\right)\left(-\frac{1}{5}\frac{\partial^2 u_0}{\partial x^2}\right)+6\left(M_{221}^{(1)}+\tilde{M}_{221}^{(1)}\right)\left(\frac{1}{5}\frac{\partial^2 \psi_0}{\partial x^2}\right)\\
&-\left(Y_{12}+\tilde{Y}_{12}\right)\frac{1}{2}\left(\frac{\partial \psi_0}{\partial x}+\frac{\partial^2 w_0}{\partial x^2}\right)\}\,\mathrm{dx}\\
&+\frac{1}{2}\int_0^L\int_A \{D_z\left(\beta\sin\left(\beta z\right)\varphi_E+\frac{2V_E}{h}\right)-D_x\cos\left(\beta z\right)\left(\frac{\partial \varphi_E}{\partial x}\right)\}dA\,dx\\
&+\frac{1}{2}\int_0^L\int_A \{B_z\left(\beta\sin\left(\beta z\right)\Upsilon_H+\frac{2\Omega_H}{h}\right)-B_x\cos\left(\beta z\right)\left(\frac{\partial \Upsilon_H}{\partial x}\right)\}dA\,dx
\end{aligned} \tag{32}$$

The normal stress resultant force $\left(N,\tilde{N}\right)$, bending moments $\left(M,\tilde{M}\right)$, couple moment $\left(Y_{12},\tilde{Y_{12}}\right)$ and other higher-order resultant force and moment can be expressed in Appendix A [43-45].

The total kinetic energies for MEE micro-beam contain of bulk kinetic energy k^b and surface kinetic energy k^s can be calculated from:

$$\begin{aligned}
k^b+k^s &= \frac{1}{2}\int_0^L\left\{(\rho\,\mathrm{I}_0+\rho_s\,\tilde{\mathrm{I}}_0)\left(\left(\frac{\partial u_0}{\partial t}\right)^2+\left(\frac{\partial w_0}{\partial t}\right)^2\right)+(\rho\,\mathrm{I}_2+\rho_s\,\tilde{\mathrm{I}}_2)\left(\frac{\partial \psi_0}{\partial t}\right)^2\right\}dx\\
\mathrm{I}_0 &= \int_A dA,\tilde{\mathrm{I}}_0=\int_S dS,\mathrm{I}_2=\int_A z^2dA,\tilde{\mathrm{I}}_2=\int_S z^2dS
\end{aligned} \tag{33}$$

The work done by the external force including the external magnetic potential Ω_H, external electric potential V_E and temperature change ΔT can be calculated as follows:

$$\begin{aligned}
V_{external} &= \frac{1}{2}\int_0^L\left((N_m+N_e+N_t)\left(\frac{\partial}{\partial x}w_0\right)^2\right)dx\\
N_m &= -2\tilde{q}_{31}\Omega_H,N_e=-2\tilde{e}_{31}V_E,N_t=\tilde{\beta}_1 h\Delta T
\end{aligned} \tag{34}$$

The work due to elastic foundation can be obtained as follows:

$$V_{elastic\ medium}=-\frac{1}{2}\int_0^L[(k_w w_0-k_g\nabla^2 w_0)w_0]dx \tag{35}$$

where k_w is the spring constant of the Winkler type and k_g represents the shear constant of the Pasternak type.

The work done due to moving nano-particle can be written as [46]:

$$V_{Particle}=\frac{1}{2}\int_0^L[(\frac{m_c}{b}\delta(\mathrm{x}-\mathrm{x}_p))\frac{\partial^2 w_0}{\partial t^2}]w_0 dx \tag{36}$$

where m_c, x_p, b and x are the nano-particle mass, the location of nano-particle, the width of micro-beam and the impulse function, respectively. The Dirac-delta function for the moving nano-particle is defined as follows [46-47]:

$$\int_{x_1}^{x_2} g(\mathrm{x})\delta^n(\mathrm{x}-\mathrm{x}_p)\,\mathrm{dx}=\begin{cases}(-1)^n g^n(\mathrm{x}_p) & \mathrm{x}_1<\mathrm{x}_p<\mathrm{x}_2\\ 0 & otherwise\end{cases} \tag{37}$$

where $\delta^n(x)$ denotes nth derivative of Dirac-delta function.

Hamilton's principle for MEE micro-beam is used to derive the governing equations of motions as follows:

$$\int_{t_0}^{t_1}\delta U^b+\delta U^s-\delta k^b-\delta k^s-\delta V_{external}-\delta V_{elastic\ medium}-\delta V_{particle}=0 \tag{38}$$

Substituting Eqs. (31) - (36) into Eq. (38), the following equations of motion can be derived as:

$$\begin{aligned}
&\delta u_0:\\
&-\frac{\partial\left(\mathrm{N}+\tilde{\mathrm{N}}\right)}{\partial x}+\frac{\partial^2\left(P_1+\tilde{P}_1\right)}{\partial x^2}+\frac{2}{5}\frac{\partial^2\left(T_{111}^{(1)}+\tilde{T}_{111}^{(1)}\right)}{\partial x^2}-\frac{6}{5}\frac{\partial^2\left(T_{221}^{(1)}+\tilde{T}_{221}^{(1)}\right)}{\partial x^2}+\left(\rho I_0+\rho_s\tilde{I}_0\right)\frac{\partial^2 u_0}{\partial t^2}=0\\
&\delta w_0:\\
&-\frac{\partial Q}{\partial x}-\frac{1}{5}\frac{\partial^2 T_{333}^{(1)}}{\partial x^2}+\frac{4}{5}\frac{\partial^2 T_{113}^{(1)}}{\partial x^2}-\frac{1}{5}\frac{\partial^2 T_{223}^{(1)}}{\partial x^2}-\frac{1}{2}\frac{\partial^2\left(Y_{12}+\tilde{Y}_{12}\right)}{\partial x^2}+(N_m+N_e+N_t)\frac{\partial^2 w_0}{\partial x^2}\\
&+(k_w w_0-k_g\nabla^2 w_0)+(\frac{m_c}{b}\delta(\mathrm{x}-\mathrm{x}_{mp}))(\frac{\partial^2 w_0}{\partial t^2})+\left(\rho I_0+\rho_s\tilde{I}_0\right)\frac{\partial^2 w_0}{\partial t^2}=0\\
&\delta\psi_0:\\
&\frac{\partial\left(M+\tilde{M}\right)}{\partial x}-Q+\frac{\partial\left(P_3+\tilde{P}_3\right)}{\partial x}-\frac{\partial^2\left(M_1^{(1)}+\tilde{M}_1^{(1)}\right)}{\partial x^2}-\frac{2}{5}\frac{\partial^2\left(M_{111}^{(1)}+\tilde{M}_{111}^{(1)}\right)}{\partial x^2}\\
&-\frac{2}{5}\frac{\partial T_{333}^{(1)}}{\partial x}-\frac{1}{5}\frac{\partial\tilde{T}_{333}^{(1)}}{\partial x}+\frac{8}{5}\frac{\partial T_{113}^{(1)}}{\partial x}+\frac{4}{5}\frac{\partial\tilde{T}_{113}^{(1)}}{\partial x}-\frac{2}{5}\frac{\partial T_{223}^{(1)}}{\partial x}-\frac{1}{5}\frac{\partial\tilde{T}_{223}^{(1)}}{\partial x}\\
&+\frac{6}{5}\frac{\partial^2\left(M_{221}^{(1)}+\tilde{M}_{221}^{(1)}\right)}{\partial x^2}+\frac{1}{2}\frac{\partial\left(Y_{12}+\tilde{Y}_{12}\right)}{\partial x}+\left(\rho I_2+\rho_s\tilde{I}_2\right)\frac{\partial^2\psi_0}{\partial t^2}=0\\
&\delta\varphi_E:\\
&\int_A(\frac{\partial D_x}{\partial x}\cos(\beta z)+D_z\beta\sin(\beta z))dA=0\\
&\delta\Upsilon_H:\\
&\int_A(\frac{\partial B_x}{\partial x}\cos(\beta z)+B_z\beta\sin(\beta z))dA=0
\end{aligned} \tag{39}$$

Substituting Appendix (A.2) into Eq. (39), the governing equations of motion can be obtained as follows:

$$
\begin{aligned}
&\delta u_0 :\\
&-(\mathrm{A}_{11}+\tilde{\mathrm{A}}_{11})\frac{\partial^2 u_0}{\partial x^2}+(\mathrm{A}_{55}+\tilde{\mathrm{A}}_{55})(2l_0{}^2+\frac{4}{5}l_1{}^2)\frac{\partial^4 u_0}{\partial x^4}+\left(\rho I_0+\rho_s\tilde{I}_0\right)\frac{\partial^2 u_0}{\partial t^2}=0\\
&\delta w_0 :\\
&-(\mathrm{A}_{44})\frac{\partial^2 w_0}{\partial x^2}+(\mathrm{A}_{44})\frac{\partial \psi_0}{\partial x}-(\frac{16}{15}l_1{}^2A_{55}-\frac{1}{4}l_2{}^2(\mathrm{A}_{55}+\tilde{\mathrm{A}}_{55}))\frac{\partial^3 \psi_0}{\partial x^3}+(E_{15})\frac{\partial \varphi_E}{\partial x}\\
&+(\frac{8}{15}l_1{}^2A_{55}+\frac{1}{4}l_2^2(\mathrm{A}_{55}+\tilde{\mathrm{A}}_{55}))\frac{\partial^4 w_0}{\partial x^4}+(N_m+N_e+N_t)\frac{\partial^2 w_0}{\partial x^2}+(Q_{15})\frac{\partial \Upsilon_H}{\partial x}\\
&+(k_w w_0-k_g\nabla^2 w_0)+(\frac{m_c}{b}\delta(\mathrm{x}-\mathrm{x}_{mp}))(\frac{\partial^2 w_0}{\partial t^2})+\left(\rho I_0+\rho_s\tilde{I}_0\right)\frac{\partial^2 w_0}{\partial t^2}=0\\
&\delta\psi_0 :\\
&(2l_0{}^2+\frac{4}{5}l_1{}^2)(\mathrm{I}_3+\tilde{\mathrm{I}}_3)\frac{\partial^4 \psi_0}{\partial x^4}-(A_{44})\frac{\partial w_0}{\partial x}+(A_{44})\psi_0\\
&-(\frac{32}{15}l_1{}^2\,\mathrm{A}_{55}+\frac{8}{15}l_1{}^2\,\tilde{\mathrm{A}}_{55}+\frac{1}{4}l_2{}^2(\mathrm{A}_{55}+\tilde{\mathrm{A}}_{55})+2l_0{}^2(\mathrm{A}_{55}+\tilde{\mathrm{A}}_{55})+\mathrm{D}_{11}+\tilde{\mathrm{D}}_{11})\frac{\partial^2 \psi_0}{\partial x^2}\\
&+(\frac{16}{15}l_1{}^2\,\mathrm{A}_{55}-\frac{1}{4}l_2{}^2(\mathrm{A}_{55}+\tilde{\mathrm{A}}_{55}))\frac{\partial^3 w_0}{\partial x^3}+(E_{15}+E_{31}+\tilde{E}_{31})\frac{\partial \varphi_E}{\partial x}\\
&+(Q_{15}+Q_{31}+\tilde{Q}_{31})\frac{\partial \Upsilon_H}{\partial x}+\left(\rho I_2+\rho_s\tilde{I}_2\right)\frac{\partial^2 \psi_0}{\partial t^2}=0\\
&\delta\varphi_E :\\
&-E_{31}\frac{\partial \psi_0}{\partial x}+E_{15}(\frac{\partial^2 w_0}{\partial x^2}-\frac{\partial \psi_0}{\partial x})+X_{11}\frac{\partial^2 \varphi_E}{\partial x^2}+Y_{11}\frac{\partial^2 \Upsilon_H}{\partial x^2}-X_{33}\varphi_E-Y_{33}\Upsilon_H=0\\
&\delta\Upsilon_H :\\
&-Q_{31}\frac{\partial \psi_0}{\partial x}+Q_{15}(\frac{\partial^2 w_0}{\partial x^2}-\frac{\partial \psi_0}{\partial x})+Y_{11}\frac{\partial^2 \varphi_E}{\partial x^2}+T_{11}\frac{\partial^2 \Upsilon_H}{\partial x^2}-Y_{33}\varphi_E-T_{33}\Upsilon_H=0
\end{aligned}
\tag{40}
$$

where the constants of Eq. (40) are defined in Appendix A.

The dimensionless parameters for magneto-electro-elastic Timoshenko micro beam model based on surface stress effect and MSGT under moving nano-particle are defined as follows:

$$
\begin{aligned}
&X=\frac{x}{L},\ (\mathrm{u}_0,\mathrm{w}_0)=\frac{(\mathrm{U},\mathrm{W})}{h},\psi_0=\Psi,\Phi=\frac{\varphi_E}{\varphi_0},\Theta=\frac{\Upsilon_H}{\Upsilon_0},\varphi_0=\sqrt{\frac{A_{11}}{X_{33}}},\Upsilon_0=\sqrt{\frac{A_{11}}{T_{33}}}\\
&\tau=\frac{t}{L}\sqrt{\frac{A_{11}}{\rho I_0}},\eta=\frac{L}{h},(\bar{\mathrm{N}}_m,\bar{\mathrm{N}}_e,\bar{\mathrm{N}}_t)=\frac{(\mathrm{N}_m,\mathrm{N}_e,\mathrm{N}_t)}{A_{11}},(\mathrm{I}_{110},\tilde{\mathrm{I}}_{110})=\frac{(\rho\,\mathrm{I}_0,\rho_s\,\tilde{\mathrm{I}}_0)}{\rho\,\mathrm{I}_0}\\
&(\mathrm{I}_{220},\tilde{\mathrm{I}}_{220})=\frac{(\rho\,\mathrm{I}_2,\rho_s\,\tilde{\mathrm{I}}_2)}{\rho\,\mathrm{I}_2},(\mathrm{I}_{33},\tilde{\mathrm{I}}_{33})=\frac{(\mathrm{I}_3,\tilde{\mathrm{I}}_3)}{A_{11}h^2},(\mathrm{a}_{11},\mathrm{a}_{55},\mathrm{a}_{44},\tilde{\mathrm{a}}_{11},\tilde{\mathrm{a}}_{55},\tilde{\mathrm{a}}_{44})=\frac{(\mathrm{A}_{11},A_{55},A_{44},\tilde{\mathrm{A}}_{11},\tilde{A}_{55},\tilde{A}_{44})}{A_{11}}\\
&(\mathrm{d}_{11},\tilde{\mathrm{d}}_{11})=\frac{(D_{11},\tilde{D}_{11})}{A_{11}h^2},(\bar{\mathrm{k}}_w,\bar{\mathrm{k}}_g)=(\frac{\mathrm{k}_w L^2}{A_{11}},\frac{\mathrm{k}_g}{A_{11}}),\bar{\mathrm{m}}_c=\frac{m_c}{\rho\,\mathrm{I}_0 b},(\ell_0,\ell_1,\ell_2)=\frac{(\mathrm{l}_0,\mathrm{l}_1,\mathrm{l}_2)}{h}\\
&(\hat{\mathrm{E}}_{15},\hat{\mathrm{E}}_{31},\hat{\tilde{\mathrm{E}}}_{31})=(\frac{E_{15}\varphi_0}{A_{11}h},\frac{E_{31}\varphi_0}{A_{11}h},\frac{\tilde{E}_{31}\varphi_0}{A_{11}h}),(\hat{Q}_{15},\hat{\mathrm{Q}}_{31},\hat{\tilde{\mathrm{Q}}}_{31})=(\frac{Q_{15}\Upsilon_0}{A_{11}h},\frac{Q_{31}\Upsilon_0}{A_{11}h},\frac{\tilde{Q}_{31}\Upsilon_0}{A_{11}h})\\
&,(\hat{\mathrm{X}}_{11},\hat{X}_{33})=(\frac{X_{11}\varphi_0^2}{A_{11}h^2},\frac{X_{33}\varphi_0^2}{A_{11}})\\
&(\hat{T}_{11},\hat{\mathrm{T}}_{33})=(\frac{T_{11}\Upsilon_0^2}{A_{11}h^2},\frac{T_{33}\Upsilon_0^2}{A_{11}}),(\hat{\mathrm{Y}}_{11},\hat{\mathrm{Y}}_{33})=(\frac{Y_{11}\Upsilon_0\varphi_0}{A_{11}h^2},\frac{Y_{33}\Upsilon_0\varphi_0}{A_{11}})
\end{aligned}
\tag{41}
$$

Using Eq. (41), the dimensionless governing equations of motion can be written as:

$$\delta U:$$

$$-(a_{11}+\tilde{a}_{11})\eta^2\frac{\partial^2 U}{\partial X^2}+(a_{55}+\tilde{a}_{55})(2\ell_0{}^2+\frac{4}{5}\ell_1{}^2)\frac{\partial^4 U}{\partial X^4}+\left(I_{110}+\tilde{I}_{110}\right)\eta^2\frac{\partial^2 U}{\partial \tau^2}=0$$

$$\delta W:$$

$$-(\mathrm{a}_{44})\eta^2\frac{\partial^2 W}{\partial X^2}+(\mathrm{a}_{44})\eta^3\frac{\partial \Psi}{\partial X}-(\frac{16}{15}\ell_1{}^2 a_{55}-\frac{1}{4}\ell_2{}^2(\mathrm{a}_{55}+\tilde{a}_{55}))\eta\frac{\partial^3 \Psi}{\partial X^3}+(\hat{E}_{15})\eta^2\frac{\partial^2 \Phi}{\partial X^2}$$

$$+(\frac{8}{15}\ell_1{}^2 a_{55}+\frac{1}{4}\ell_2^2(\mathrm{a}_{55}+\tilde{a}_{55}))\frac{\partial^4 W}{\partial X^4}+(\bar{N}_m+\bar{N}_e+\bar{N}_t)\eta^2\frac{\partial^2 W}{\partial X^2}+(\hat{Q}_{15})\eta^2\frac{\partial^2 \Theta}{\partial X^2}$$

$$+(\bar{k}_w W-\bar{k}_g\nabla^2 W)\eta^2+(\bar{m}_c\eta^2)(\frac{\partial^2 W}{\partial \tau^2})+\left(I_{110}+\tilde{I}_{110}\right)\eta^2\frac{\partial^2 w_0}{\partial \tau^2}=0$$

$$\delta\Psi:$$

$$(2\ell_0{}^2+\frac{4}{5}\ell_1{}^2)(\mathrm{I}_{33}+\tilde{\mathrm{I}}_{33})\frac{\partial^4 \Psi}{\partial X^4}-(a_{44})\eta^3\frac{\partial W}{\partial X}+(\mathrm{a}_{44})\eta^4\Psi$$

$$-(\frac{32}{15}\ell_1{}^2 a_{55}+\frac{8}{15}\ell_1{}^2\tilde{a}_{55}+\frac{1}{4}\ell_2{}^2(\mathrm{a}_{55}+\tilde{a}_{55})+2\ell_0{}^2(\mathrm{a}_{55}+\tilde{a}_{55})+d_{11}+\tilde{d}_{11})\eta^2\frac{\partial^2 \Psi}{\partial X^2} \tag{42}$$

$$+(\frac{16}{15}\ell_1{}^2 a_{55}-\frac{1}{4}\ell_2{}^2(\mathrm{a}_{55}+\tilde{a}_{55}))\eta\frac{\partial^3 W}{\partial X^3}+(\hat{E}_{15}+\hat{E}_{31}+\hat{\tilde{E}}_{31})\eta^3\frac{\partial \Phi}{\partial X}$$

$$+(\hat{Q}_{15}+\hat{Q}_{31}+\hat{\tilde{Q}}_{31})\eta^3\frac{\partial \Theta}{\partial X}+\left(I_{220}+\tilde{I}_{220}\right)\eta^2\frac{\partial^2 \Psi}{\partial \tau^2}=0$$

$$\delta\Phi:$$

$$-\hat{E}_{31}\eta\frac{\partial \Psi}{\partial X}+\hat{E}_{15}(\frac{\partial^2 W}{\partial X^2}-\eta\frac{\partial \Psi}{\partial X})+\hat{X}_{11}\frac{\partial^2 \Phi}{\partial X^2}+\hat{Y}_{11}\frac{\partial^2 \Theta}{\partial X^2}-\hat{X}_{33}\eta^2\Phi-\hat{Y}_{33}\eta^2\Theta=0$$

$$\delta\Theta:$$

$$-\hat{Q}_{31}\eta\frac{\partial \Psi}{\partial X}+\hat{Q}_{15}(\frac{\partial^2 W}{\partial X^2}-\eta\frac{\partial \Psi}{\partial X})+\hat{Y}_{11}\frac{\partial^2 \Phi}{\partial X^2}+\hat{T}_{11}\frac{\partial^2 \Theta}{\partial X^2}-\hat{Y}_{33}\eta^2\Phi-\hat{T}_{33}\eta^2\Theta=0$$

The dimensionless simply supported (S-S) boundary conditions for MEE are considered as follows:

$$U=W=\frac{\partial \Psi}{\partial X}=\Phi=\Theta=0,\quad \frac{\partial^2 W}{\partial X^2}=0\quad at\ (\mathrm{X}=0,1) \tag{43}$$

3 DIFFERENTIAL QUADRATURE METHOD

In this section, differential quadrature method (DQM) is utilized to solve the governing equations of motion. This technique is numerical method which approximates the spatial derivatives of a function at a particular sampling point as a weighted linear sum of the function values at all sampling points chosen in a specified direction. According to this method, the function *f* and derivatives are approximates as [48-49]:

$$\left.\frac{d^n f}{dx^n}\right|_{x=x_i}=\sum_{j=1}^{N}C_{ij}^{(n)}f(\mathrm{x}_j) \tag{44}$$

where *f* can be taken as U, W, Ψ, Φ and Θ. $C_{ij}^{(\mathrm{n})}$ and *N* are the weighting coefficients matrix and number of grid point respectively. To determine the unequally spaced position of the grid points the Chebyshev–Gauss–Lobatto polynomials was employed as follow [50]:

$$x_i = \frac{L}{2}\left[1-\cos\left(\frac{2i-1}{N-1}\right)\pi\right] \tag{45}$$

Using Eqs. (42) and (43), a set of linear ordinary differential equations and boundary conditions are obtained that are written in Appendix B. Using Eqs. (B.1)- (B.2), a set of nonlinear homogenous partially differential equations are obtained which in matrix form can be expressed as follows:

$$([\mathrm{K}]\{X\}+[M]\{\ddot{X}\})=\{0\} \tag{46}$$

where $[\mathrm{K}],[M]$ are the stiffness and mass matrices, respectively and $\{X\}$ denotes displacements vector as:

$$\{X\}=\left\{\{U\}^T,\{W\}^T,\{\Psi\}^T,\{\Phi\}^T,\{\Theta\}^T\right\}^T \tag{47}$$

General solution of motion equations is considered as follows:

$$\begin{aligned}
&\mathrm{U}(x,t)=\hat{U}(X)\,\mathrm{e}^{i\omega\tau}\\
&\mathrm{W}(x,t)=\hat{W}(X)\,\mathrm{e}^{i\omega\tau}\\
&\Psi(x,t)=\hat{\Psi}(X)\,\mathrm{e}^{i\omega\tau}\\
&\Phi(x,t)=\hat{\Phi}(X)\,\mathrm{e}^{i\omega\tau}\\
&\Theta(x,t)=\hat{\Theta}(X)\,\mathrm{e}^{i\omega\tau}
\end{aligned} \tag{48}$$

where $\omega=\sqrt{\frac{\rho I_0}{A_{11}}}\Omega L$ is the dimensionless natural frequency and, Ω and ρ denote the fundamental natural frequency and the density of micro-beam, respectively. Substituting Eq. (46) into Eq. (47) yields the linear eigenvalue equations as follows:

$$([\mathrm{K}]-[M]\omega^2)\{X\}=\{0\} \tag{49}$$

By solving Eq. (49), the dimensionless natural frequencies ω and their associated vibration mode shapes can be extracted.

4 NUMERICAL RESULTS AND DISCUSSION

The presented results are based on the following data for geometry of MEE micro-beam [51-52]. Also the material properties of BiTiO3–CoFe2O4 can be stated as follows [14]:

$$1=17.6\mu m, h=2l, b=2h, \mathrm{L}=10h \tag{50}$$

First, the effect of the grid point numbers on the accuracy and convergence of analysis is studied. In this regard the dimensionless fundamental natural frequency versus number of total discrete grid points N is illustrated in Fig. 2. Thus, the number of grid points for convergence and acceptable accuracy of the results is selected to be N>=15. It should be noted that all of represented results are based on Eq. (50), the data of each Table or Figure stated under them. To check the accuracy of the present work, the obtained results are compared with the analytical solutions given by Ansari et al. [53] in Table 1. This Table gives the dimensionless natural frequencies for the simply supported Timoshenko micro-beam and different theories. A good agreement is found between the present results and those of analytical solutions.

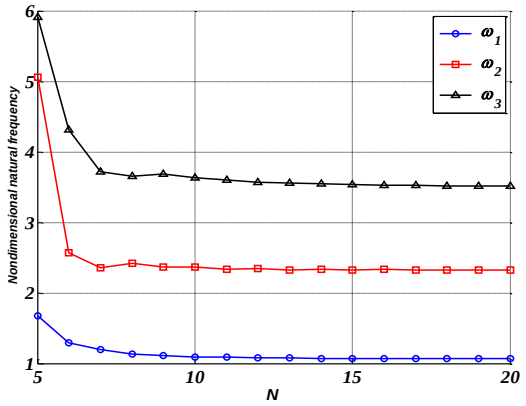

Fig.2
Dimensionless natural frequency versus number of grid points $\left(k_w = k_g = V_E = \Omega_H = \Delta T = m_c = \rho_s = c_{11}^s = e_{31}^s = q_{31}^s = 0\right)$.

Table1
The comparison between the present work and the obtained results by Ansari et al. [53] for simply supported Timoshenko micro-beam based on various size dependent theories. ($1 = 15\mu m, \nu = 0.17, \mathrm{E} = 427GPa, \rho = 3100\frac{kg}{m^3}$).

Ceramic material	Strain gradient theory(SGT) $\left(l_0 = l_1 = l_2 = l\right)$	Modified couple stress theory(MCST) $\left(l_0 = l_1 = 0, l_2 = l\right)$	Classical theory(CT) $\left(l_0 = l_1 = l_2 = 0\right)$
Ansari [53]	1.2608	0.8538	0.5776
Present work	1.2667	0.8573	0.6063

Fig.3 shows the rotation angle versus length of MEE micro-beam for various material length scale parameters based on the modified strain gradient theory and simply supported boundary conditions. It is seen that by increasing the value of $\frac{h}{l}$, the values of the rotation angle for MEE micro-beam increases. Also, the rotation angle is symmetric and at $\frac{X}{L} = 0.5$ the value of rotation angle varies from negative to positive along length of the micro-beam.

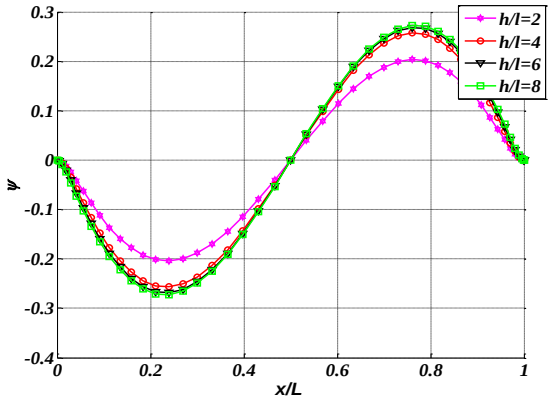

Fig.3
The rotation angle versus length of MEE composite micro-beam for various material length scale parameters.
$\left(k_w = k_g = V_E = \Omega_H = \Delta T = m_c = \rho_s = c_{11}^s = e_{31}^s = q_{31}^s = 0\right)$

The effect of material length scale parameter on the dimensionless electric potential for MEE Timoshenko micro beam model is illustrated in Fig.4 that maximum electric potential is occurred at midline simply supported MEE micro-beam and by increasing the value of $\frac{h}{l}$, the value of dimensionless electric potential decreases at 0.3-0.7 ranges.

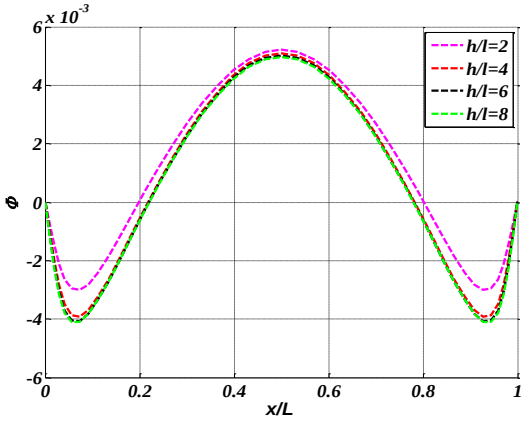

Fig.4
The effect of material length scale parameter on the dimensionless electric potential for MEE micro composite Timoshenko beam model.
$\left(k_w = k_g = V_E = \Omega_H = \Delta T = m_c = \rho_s = c_{11}^s = e_{31}^s = q_{31}^s = 0\right)$

Fig.5 depicts dimensionless magnetic parameter for different material length scale parameters based on modified strain gradient model. It is observed that by increasing value of $\frac{h}{l}$ increases the dimensionless magnetic parameter.

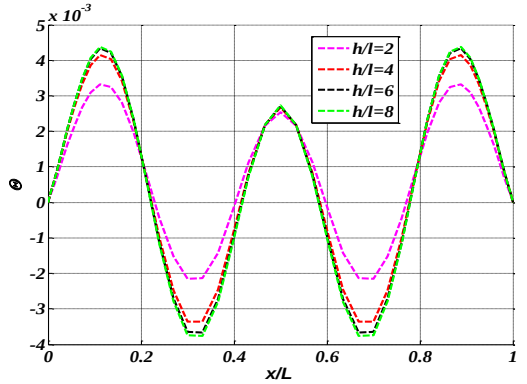

Fig.5
The effect of material length scale parameter on the dimensionless magnetic parameter for MEE micro composite Timoshenko beam model.
$\left(k_w = k_g = V_E = \Omega_H = \Delta T = m_c = \rho_s = c_{11}^s = e_{31}^s = q_{31}^s = 0\right)$

Figs. 6, 7 and 8 present the effect of electric potential and magnetic parameter simultaneously on the dimensionless fundamental natural frequency based on modified strain gradient (MSGT), modified couple stress (MCST) and classical theories (CT), respectively. It can be seen that the effect of electric potential and magnetic parameter simultaneously increases the dimensionless natural frequency. On the other hands, with considering two parameters, the stiffness of MEE Timoshenko micro beam model increases. It can be seen that the stiffness of micro structure increases by MSGT is more than MCST and CT. Moreover, the dimensionless natural frequency based on MSGT is more than two other theories.

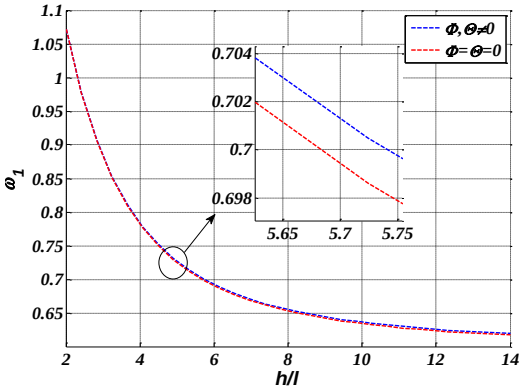

Fig.6
The influence of dimensionless electric potential and magnetic parameter on dimensionless first natural frequency for MEE composite micro-beam based on modified strain gradient model.
$\left(k_w = k_g = V_E = \Omega_H = \Delta T = m_c = \rho_s = c_{11}^s = e_{31}^s = q_{31}^s = 0\right)$

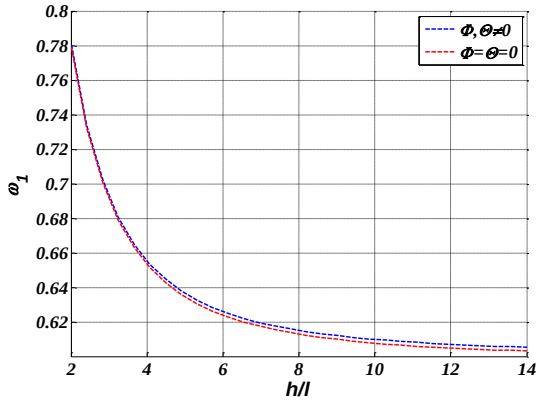

Fig.7
The influence of dimensionless electric potential and magnetic parameter on dimensionless first natural frequency for MEE composite micro-beam based on modified couple stress theory.
$\left(k_w = k_g = V_E = \Omega_H = \Delta T = m_c = \rho_s = c_{11}^s = e_{31}^s = q_{31}^s = l_0 = l_1 = 0, l_2 = l\right)$

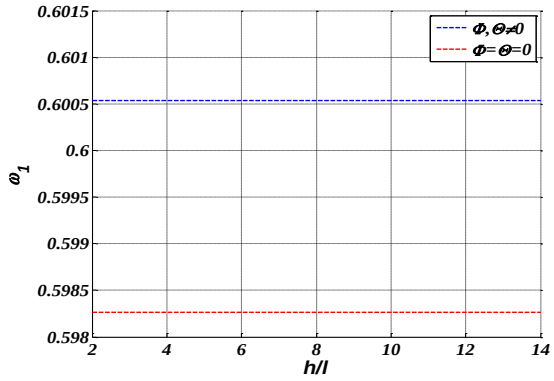

Fig.8
The influence of dimensionless electric potential and magnetic parameter on dimensionless first natural frequency for MEE composite micro-beam based on classical theory.
$\left(k_w = k_g = V_E = \Omega_H = \Delta T = m_c = \rho_s = c_{11}^s = e_{31}^s = q_{31}^s = l_0 = l_1 = l_2 = 0\right)$

The effect of the external electric voltage and external magnetic parameter on the dimensionless fundamental natural frequency of the micro-beam based on MSGT is illustrated in Figs. 9 and 10, respectively. It is shown from this figure that with increasing slenderness ratio, the dimensionless fundamental natural frequency decreases. Also, the influence of the external electric voltage and external magnetic parameter on the dimensionless frequency for Timoshenko micro beam model in higher slenderness ratios is more. Also, it is realized from Fig. 9 that the dimensionless natural frequency of the MEE micro-beam decreases with increasing the external electric voltage for strain gradient theory. However, it is concluded from Fig. 10 that by increasing the external magnetic parameter, the dimensionless natural frequency of the MEE micro-beam increases.

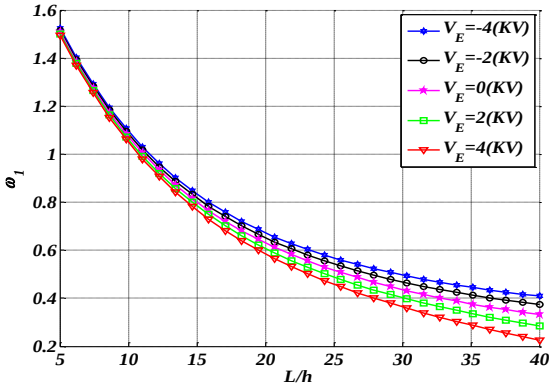

Fig.9
The effect of external electric voltage on the dimensionless fundamental natural frequency based on MSGT.
$\left(k_w = k_g = \Omega_H = \Delta T = m_c = \rho_s = c_{11}^s = e_{31}^s = q_{31}^s = 0\right)$

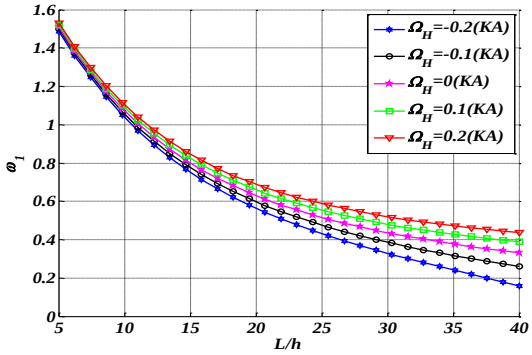

Fig.10
The effect of external magnetic parameter on the dimensionless fundamental natural frequency based on MSGT.
$\left(k_w = k_g = V_E = \Delta T = m_c = \rho_s = c_{11}^s = e_{31}^s = q_{31}^s = 0\right)$

Figs. 11(a) and 11(b) show the effect of two parameters elastic foundation on the dimensionless electric potential based on MSGT. It is seen that with increasing elastic foundation, the electric potential decreases.

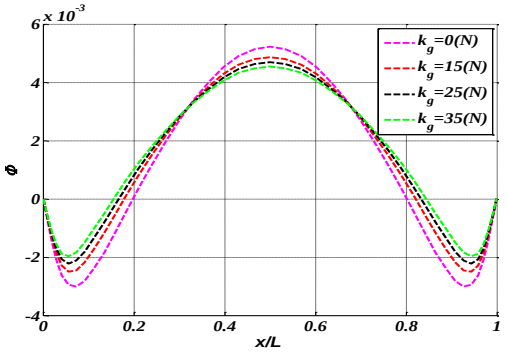

(a)

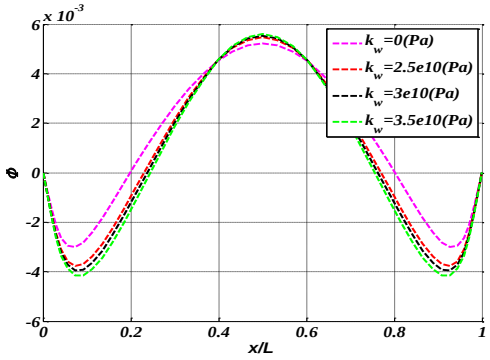

(b)

Fig.11
a) The effect of shear Pasternak constant on the dimensionless electric potential based on MSGT.
$\left(k_w = V_E = \Omega_H = \Delta T = m_c = \rho_s = c_{11}^s = e_{31}^s = q_{31}^s = 0\right)$
b) The effect of spring Winkler constant on the dimensionless electric potential based on MSGT.
$\left(k_g = V_E = \Omega_H = \Delta T = m_c = \rho_s = c_{11}^s = e_{31}^s = q_{31}^s = 0\right)$

Figs. 12(a) and 12(b) depict the effect of two parameters elastic foundation on magnetic parameter based on MSGT. It is concluded that the magnetic parameter increases with an increase in the elastic foundation.

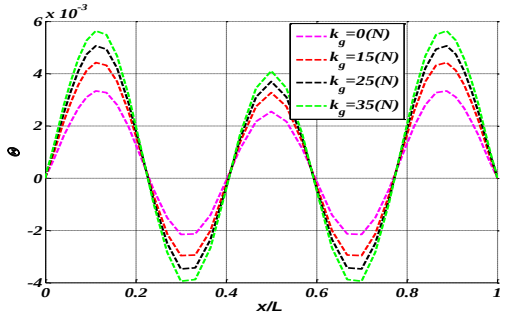

(a)

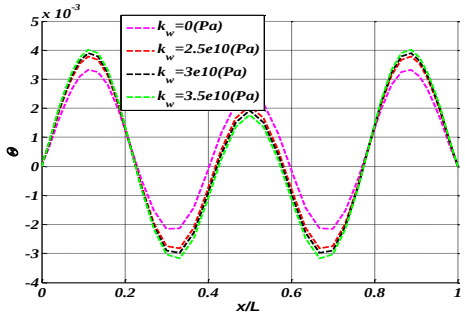

(b)

Fig.12
a) The effect of shear Pasternak constant on the dimensionless magnetic parameter based on MSGT.
$\left(k_w = V_E = \Omega_H = \Delta T = m_c = \rho_s = c_{11}^s = e_{31}^s = q_{31}^s = 0\right)$
b) The effect of spring Winkler constant on the dimensionless magnetic parameter based on MSGT.
$\left(k_g = V_E = \Omega_H = \Delta T = m_c = \rho_s = c_{11}^s = e_{31}^s = q_{31}^s = 0\right)$

Fig. 13 illustrates the effect of nano particle mass on dimensionless natural frequency based on MSGT. It is assumed that the nano particle is placed at $x_P = \frac{L}{2}$. It is found that by increasing the mass of nano-particle, the dimensionless natural frequency of system decreases.

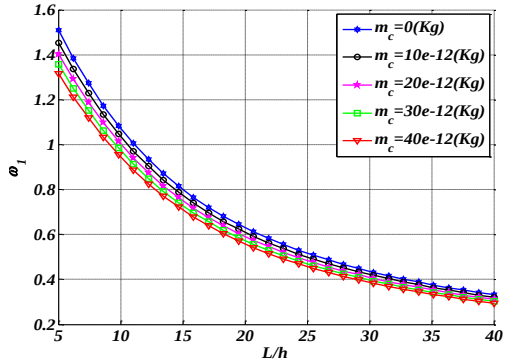

Fig.13
The effect of nano particle mass on dimensionless natural frequency based on MSGT.
$\left(k_g = k_w = V_E = \Omega_H = \Delta T_c = \rho_s = c_{11}^s = e_{31}^s = q_{31}^s = 0\right)$

Table 2. shows the effect of temperature change on dimensionless first three natural frequencies based on various size dependent theories such as MSGT, MCST and CT. It can be seen that with an increase in the temperature change, dimensionless natural frequency of micro beam model decreases. Also with increasing temperature change the stiffness of micro-beam decreases. According to Ghorbanpour Arani et al. [54], the mechanical and electrical properties for surface stress effect are defined as follows:

$$\rho_s = 5.61e-6\frac{kg}{m^2}, c_{11}^s = 44.2\frac{N}{m} \text{ and } e_{31}^s = 0.216\frac{nC}{m}, q_{31}^s = 3e-5\frac{N}{m} \tag{51}$$

Using the data of Eq. (51), Table 3. shows the surface stress effect on dimensionless first three natural frequencies of MEE micro-beam for different values of slenderness ratio ($\frac{L}{h}$) based on MSGT, MCST and CT. It is concluded that by considering the surface stress effect, the dimensionless natural frequency of system decreases.

Table2
The effect of temperature change $\Delta T\,(^{\circ}\mathrm{C})$ on the dimensionless first three natural frequency based on various size dependent theories. $\left(k_g = k_w = V_E = \Omega_H = m_c = \rho_s = c_{11}^s = e_{31}^s = q_{31}^s = 0\right)$.

Various theories	mode	$\Delta T\,(^{\circ}\mathrm{C})$					
		0	40	80	120	160	200
MSGT	1	1.0722	1.0719	1.0717	1.0714	1.0711	1.0708
	2	2.3280	2.3276	2.3272	2.3267	2.3263	2.3259
	3	3.5361	3.5361	3.5361	3.5361	3.5361	3.5361
MCST	1	0.7804	0.7801	0.7797	0.7793	0.7789	0.7786
	2	1.8283	1.8278	1.8273	1.8268	1.8263	1.8258
	3	3.0703	3.0698	3.0693	3.0688	3.0683	3.0678
CT	1	0.6005	0.6000	0.5995	0.5990	0.5985	0.5980
	2	1.4041	1.4035	1.4028	1.4021	1.4015	1.4008
	3	2.3361	2.3354	2.3347	2.3340	2.3333	2.3327

Table3
Surface stress effect on the dimensionless first three natural frequencies for different values of slenderness ratio based on various size dependent theories. $\left(k_g = k_w = V_E = \Omega_H = \Delta T = m_c = 0, l = 1\mu m\right)$.

various theories	mode	With neglecting surface effect	With considering surface effect	With neglecting surface effect	With considering surface effect	With neglecting surface effect	With considering surface effect
		$L = 10h$		$L = 20h$		$L = 30h$	
MSGT	1	1.0722	1.0716	0.6302	0.6299	0.4366	0.4364
	2	2.3280	2.3262	1.5689	1.5679	1.1416	1.1410
	3	3.5361	3.5342	2.7730	2.7711	2.1048	2.1036
MCST	1	0.7804	0.7802	0.4379	0.4378	0.2997	0.2996
	2	1.8283	1.8270	1.1341	1.1336	0.8012	0.8009
	3	3.0703	3.0682	2.0722	2.0711	1.5119	1.5113
CT	1	0.6005	0.6005	0.3272	0.3271	0.2222	0.2222
	2	1.4041	1.4034	0.8519	0.8517	0.5965	0.5964
	3	2.3361	2.3350	1.5546	1.5541	1.1257	1.1255

5 CONCLUSIONS

In this research, the free vibration analysis of magneto-electro-elastic (MEE) Timoshenko micro beam model based on surface stress effect and modified strain gradient theory (MSGT) under moving nano-particle was investigated. The governing equations of motion using Hamilton's principle were derived and these equations were solved using differential quadrature method (DQM). The effects of material length scale parameters on the rotation angle, dimensionless electric potential, and dimensionless magnetic parameter were taken into account. Also, the influences of dimensionless electric potential, dimensionless magnetic parameter, material length scale parameter, external electric voltage, external magnetic parameter, slenderness ratio, temperature change, surface stress effect, spring Winkler constant, shear Pasternak constant on the dimensionless natural frequency were considered. The results of this study are listed as follows:

1. The number of grid points for convergence and acceptable accuracy of the obtained results is selected to be N>=15.
2. It is observed from the results that with an increase in the value of $\frac{h}{l}$, the values of the rotation angle for MEE micro-beam increases. Also, the rotation angle is symmetric and at $\frac{X}{L} = 0.5$ the value of rotation angle varies from negative to positive along length of the micro-beam.
3. It can be seen that the effect of electric potential and magnetic parameter simultaneously increases the dimensionless natural frequency. On the other hands, with considering two parameters, the stiffness of MEE Timoshenko micro beam model increases. It can be seen that the stiffness of micro structure increases by MSGT more than MCST and CT. Moreover, the dimensionless natural frequency based on MSGT is more than two other theories.
4. It is shown that with increasing slenderness ratio, the dimensionless fundamental natural frequency decreases. Also, the influence of the external electric voltage and external magnetic parameter on the dimensionless frequency for Timoshenko micro beam model in higher slenderness ratios is more. Also, it is found that the dimensionless natural frequency of the MEE micro-beam decreases with increasing the external electric voltage based on MSGT. However, it is concluded that by increasing the external magnetic parameter, the dimensionless natural frequency of the MEE micro-beam increases.
5. It is seen that with increasing elastic foundation, the electric potential decreases, while the stiffness of micro-beam as well as natural frequency increases.
6. It is concluded that the electric potential increases with an increase in the elastic foundation.
7. It is found that by increasing the mass of nano-particle, the dimensionless natural frequency of system decreases.

8. It is seen that with increasing of the temperature change, the dimensionless natural frequency of micro beam model decreases. Moreover with increasing temperature change the stiffness of micro-beam decreases.
9. It is concluded that by considering the surface stress effect, the dimensionless natural frequency of system decreases.

ACKNOWLEDGEMENTS

The authors would like to thank the referees for their valuable comments. Moreover, the authors are grateful to the Iranian Nanotechnology Development Committee for their financial support and also grateful to the University of Kashan for supporting this work by Grant no. 463855/12.

APPENDIX A

The constants in Eq. (30) are written as follows:

$$\begin{aligned}
&\bar{c}_{11}=c_{11}-\frac{c_{13}^2}{c_{33}},\bar{c}_{44}=c_{44},\bar{e}_{31}=e_{31}-\frac{c_{13}e_{33}}{c_{33}},\bar{e}_{15}=e_{15},\bar{q}_{31}=q_{31}-\frac{c_{13}q_{33}}{c_{33}}\\
&\bar{s}_{11}=s_{11},\bar{s}_{33}=s_{33}+\frac{e_{33}^2}{c_{33}},\bar{d}_{11}=d_{11},\bar{d}_{33}=d_{33}+\frac{e_{33}q_{33}}{c_{33}},\bar{\alpha}_{11}=\alpha_{11},\bar{\alpha}_{33}=\alpha_{33}+\frac{q_{33}^2}{c_{33}}\\
&\bar{q}_{15}=q_{15},\bar{\beta}_1=\beta_1-\frac{c_{13}\beta_3}{c_{33}},\bar{\nu}_3=\nu_3+\frac{e_{33}\beta_3}{c_{33}},\bar{\lambda}_3=\lambda_3+\frac{q_{33}\beta_3}{c_{33}}
\end{aligned} \tag{A.1}$$

In Eq. (32), the normal stress resultant force $\left(N,\tilde{N}\right)$, bending moments $\left(M,\tilde{M}\right)$, couple moment $\left(Y_{12},\tilde{Y}_{12}\right)$ and other higher-order resultant force and moment can be expressed as follows [43-45]:

$$\begin{aligned}
&N=\int_A\sigma_{xx}dA,\tilde{N}=\int_S\sigma_{xx}^s dS,\mathrm{M}=\int_A z\,\sigma_{xx}dA,\tilde{\mathrm{M}}=\int_S z\,\sigma_{xx}^s dS,Q=\int_A\sigma_{xz}dA,\\
&\begin{Bmatrix}P_1\\P_3\end{Bmatrix}=\int_A\begin{Bmatrix}P_x\\P_z\end{Bmatrix}dA,\begin{Bmatrix}\tilde{P}_1\\\tilde{P}_3\end{Bmatrix}=\int_s\begin{Bmatrix}P_x^s\\P_z^s\end{Bmatrix}dS,Y_{12}=\int_A m_{xy}dA,\tilde{Y}_{12}=\int_S m_{xy}^s dS,\\
&M_1^{(1)}=\int_A zP_x dA,\tilde{M}_1^{(1)}=\int_A zP_x^s dA,\begin{Bmatrix}\tilde{M}_{111}^{(1)}\\\tilde{M}_{221}^{(1)}\end{Bmatrix}=\int_s z\begin{Bmatrix}\tau_{111}^{(1)\mathrm{s}}\\\tau_{221}^{(1)\mathrm{s}}\end{Bmatrix}dS\\
&\begin{Bmatrix}T_{111}^{(1)}\\T_{333}^{(1)}\\T_{113}^{(1)}\\T_{223}^{(1)}\\T_{221}^{(1)}\end{Bmatrix}=\int_A\begin{Bmatrix}\tau_{111}^{(1)}\\\tau_{333}^{(1)}\\\tau_{113}^{(1)}\\\tau_{223}^{(1)}\\\tau_{221}^{(1)}\end{Bmatrix}dA,\begin{Bmatrix}\tilde{T}_{111}^{(1)}\\\tilde{T}_{333}^{(1)}\\\tilde{T}_{113}^{(1)}\\\tilde{T}_{223}^{(1)}\\\tilde{T}_{221}^{(1)}\end{Bmatrix}=\int_s\begin{Bmatrix}\tau_{111}^{(1)\mathrm{s}}\\\tau_{333}^{(1)\mathrm{s}}\\\tau_{113}^{(1)\mathrm{s}}\\\tau_{223}^{(1)\mathrm{s}}\\\tau_{221}^{(1)\mathrm{s}}\end{Bmatrix}dS,\begin{Bmatrix}M_{111}^{(1)}\\M_{221}^{(1)}\end{Bmatrix}=\int_s z\begin{Bmatrix}\tau_{111}^{(1)}\\\tau_{221}^{(1)}\end{Bmatrix}dA
\end{aligned} \tag{A.2}$$

The constants in Eq.(40) are defined as the following form:

$$\begin{aligned}
&A_{11}=\bar{c}_{11}A\ ,\tilde{A}_{11}=c_{11}^s S,A_{44}=\bar{c}_{44}A,A_{55}=\mu A\ ,\tilde{A}_{55}=\mu_s S,\mathrm{I}_3=\mu I_2,\tilde{\mathrm{I}}_3=\mu_s I_2\\
&,A=bh,S=2(\mathrm{b}+\mathrm{h}),D_{11}=\bar{c}_{11}I_2,\tilde{D}_{11}=c_{11}^s\tilde{I}_2\ ,\left\{E_{15},\mathrm{Q}_{15}\right\}=\int_A\left\{\bar{e}_{15},\bar{\mathrm{q}}_{15}\right\}\cos(\beta\,\mathrm{z})\,\mathrm{dA}\\
&\left\{\mathrm{E}_{31},\mathrm{Q}_{31}\right\}=\int_A\left\{\bar{e}_{31},\bar{\mathrm{q}}_{31}\right\}\beta\sin(\beta z)z\ \mathrm{dA},\left\{\tilde{\mathrm{E}}_{31},\tilde{\mathrm{Q}}_{31}\right\}=\int_S\left\{\bar{e}_{31},\bar{\mathrm{q}}_{31}\right\}\beta\sin(\beta z)z\ \mathrm{dS},\\
&\left\{\mathrm{X}_{11},Y_{11},T_{11}\right\}=\int_A\left\{\bar{s}_{11},\bar{d}_{11},\bar{\mu}_{11}\right\}\cos^2(\beta\,\mathrm{z})\,\mathrm{dA},\\
&\left\{\mathrm{X}_{33},Y_{33},T_{33}\right\}=\int_A\left\{\bar{s}_{33},\bar{d}_{33},\bar{\mu}_{33}\right\}[\beta\sin(\beta z)z\,]^2\,\mathrm{dA}
\end{aligned} \tag{A.3}$$

APPENDIX B

Using Eqs. (42) and (43), a set of linear ordinary differential equations are obtained as follows:

$$
\begin{aligned}
&-(a_{11}+\tilde{a}_{11})\eta^2\sum_{1}^{N}C_{ik}^{(2)}U_k+(a_{55}+\tilde{a}_{55})(2\ell_0{}^2+\frac{4}{5}\ell_1{}^2)\sum_{1}^{N}C_{ik}^{(4)}U_k\\
&+\left(I_{110}+\tilde{I}_{110}\right)\eta^2\frac{\partial^2 U}{\partial\tau^2}=0\\
&-(\mathrm{a}_{44})\eta^2\sum_{1}^{N}C_{ik}^{(2)}W_k+(\mathrm{a}_{44})\eta^3\sum_{1}^{N}C_{ik}^{(1)}\Psi_k\\
&-(\frac{16}{15}\ell_1{}^2a_{55}-\frac{1}{4}\ell_2{}^2(\mathrm{a}_{55}+\tilde{a}_{55}))\eta\sum_{1}^{N}C_{ik}^{(3)}\Psi_k+(\hat{E}_{15})\eta^2\sum_{1}^{N}C_{ik}^{(2)}\Phi_k\\
&+(\frac{8}{15}\ell_1{}^2a_{55}+\frac{1}{4}\ell_2^2(\mathrm{a}_{55}+\tilde{a}_{55}))\sum_{1}^{N}C_{ik}^{(4)}W_k\\
&+(\bar{N}_m+\bar{N}_e+\bar{N}_t)\eta^2\sum_{1}^{N}C_{ik}^{(2)}W_k+(\hat{Q}_{15})\eta^2\sum_{1}^{N}C_{ik}^{(2)}\Theta_k\\
&+(\bar{k}_w W-\bar{k}_g\nabla^2 W)\eta^2+(\bar{m}_c\eta^2)(\frac{\partial^2 W}{\partial\tau^2})+\left(I_{110}+\tilde{I}_{110}\right)\eta^2\frac{\partial^2 w_0}{\partial\tau^2}=0\\
&(2\ell_0{}^2+\frac{4}{5}\ell_1{}^2)(\mathrm{I}_{33}+\tilde{\mathrm{I}}_{33})\sum_{1}^{N}C_{ik}^{(4)}\Psi_k-(a_{44})\eta^3\sum_{1}^{N}C_{ik}^{(1)}W_k+(\mathrm{a}_{44})\eta^4\Psi\\
&-(\frac{32}{15}\ell_1{}^2a_{55}+\frac{8}{15}\ell_1{}^2\tilde{a}_{55}+\frac{1}{4}\ell_2{}^2(\mathrm{a}_{55}+\tilde{a}_{55})+2\ell_0{}^2(\mathrm{a}_{55}+\tilde{a}_{55})+d_{11}+\tilde{d}_{11})\eta^2\sum_{1}^{N}C_{ik}^{(2)}\Psi_k\\
&+(\frac{16}{15}\ell_1{}^2a_{55}-\frac{1}{4}\ell_2{}^2(\mathrm{a}_{55}+\tilde{a}_{55}))\eta\sum_{1}^{N}C_{ik}^{(3)}W_k+(\hat{E}_{15}+\hat{E}_{31}+\hat{\tilde{E}}_{31})\eta^3\sum_{1}^{N}C_{ik}^{(1)}\Phi_k\\
&+(\hat{Q}_{15}+\hat{Q}_{31}+\hat{\tilde{Q}}_{31})\eta^3\sum_{1}^{N}C_{ik}^{(1)}\Theta_k+\left(I_{220}+\tilde{I}_{220}\right)\eta^2\frac{\partial^2\Psi}{\partial\tau^2}=0\\
&-\hat{E}_{31}\eta\sum_{1}^{N}C_{ik}^{(1)}\Psi_k+\hat{E}_{15}(\sum_{1}^{N}C_{ik}^{(2)}W_k-\eta\sum_{1}^{N}C_{ik}^{(1)}\Psi_k)\\
&+\hat{X}_{11}\sum_{1}^{N}C_{ik}^{(2)}\Phi_k+\hat{Y_{11}}\sum_{1}^{N}C_{ik}^{(2)}\Theta_k-\hat{X}_{33}\eta^2\Phi-\hat{Y_{33}}\eta^2\Theta=0\\
&-\hat{Q}_{31}\eta\sum_{1}^{N}C_{ik}^{(1)}\Psi_k+\hat{Q}_{15}(\sum_{1}^{N}C_{ik}^{(2)}W-\eta\sum_{1}^{N}C_{ik}^{(1)}\Psi_k)\\
&+\hat{Y_{11}}\sum_{1}^{N}C_{ik}^{(2)}\Phi_k+\hat{T_{11}}\sum_{1}^{N}C_{ik}^{(2)}\Theta_k-\hat{Y_{33}}\eta^2\Phi-\hat{T_{33}}\eta^2\Theta=0
\end{aligned}
\tag{B.1}
$$

And for boundary conditions, one can be written as the following form:

$$
\begin{aligned}
&U_1=W_1=\frac{\partial\Psi_1}{\partial X}=\Phi_1=\Theta_1=0,\ \ \frac{\partial^2 W_1}{\partial X^2}=0 \qquad at \quad \mathrm{X}=0\\
&U_N=W_N=\frac{\partial\Psi_N}{\partial X}=\Phi_N=\Theta_N=0,\ \ \frac{\partial^2 W_N}{\partial X^2}=0 \quad at \quad \mathrm{X}=1
\end{aligned}
\tag{B.2}
$$

It should be noted that subscripts 1 and *N* return to grid point numbers.

REFERENCES

[1] Sun K.H., Kim Y.Y., 2010, Layout design optimization for magneto-electro-elastic laminate composites for maximized energy conversion under mechanical loading, *Smart Materials and Structures* **19**: 055008.

[2] Wang B.L., Niraula O.P., 2007, Transient thermal fracture analysis of transversely isotropic magneto-electro-elastic materials, *Journal of Thermal Stresses* **30**: 297-317.
[3] Priya S., Islam R., Dong S., Viehland D., 2007, Recent advancements in magneto-electric particulate and laminate composites, *Journal of Electroceramics* **19**: 149-166.
[4] Zhai J., Xing Z., Dong S., Li J., Viehland D., 2008, Magnetoelectric laminate composites: an overview, *Journal of the American Ceramic Society* **91**: 351-358.
[5] Nan C.W., Bichurin M., Dong S., Viehland D., Srinivasan G., 2008, Multiferroic magnetoelectric composites: historical perspective, status, and future directions, *Journal of Applied Physics* **103**: 031101.
[6] Bhangale R.K., Ganesan N., 2006, Free vibration of functionally graded non-homogeneous magneto-electro-elastic cylindrical shell, *International Journal for Computational Methods in Engineering Science and Mechanics* **7**: 191-200.
[7] Lang Z., Xuewu L., 2013, Buckling and vibration analysis of functionally graded magneto-electro-thermo-elastic circular cylindrical shells, *Applied Mathematical Modelling* **37**: 2279-2292.
[8] Razavi S., Shooshtari A., 2015, Nonlinear free vibration of magneto-electro-elastic rectangular plates, *Composite Structures* **119**: 377-384.
[9] Ke L.L., Wang Y.S., Yang J., Kitipornchai S., 2014, Free vibration of size-dependent magneto-electro-elastic nanoplates based on the nonlocal theory, *Acta Mechanica Sinica* **30**: 516-525.
[10] Li Y.S., Cai Z.Y., Shi S.Y., 2014, Buckling and free vibration of magneto-electro-elastic nanoplate based on nonlocal theory, *Composite Structures* **111**: 522-529.
[11] Shooshtari A., Razavi S., 2015, Linear and nonlinear free vibration of a multilayered magneto-electro-elastic doubly-curved shell on elastic foundation, *Composite Part B* **78**: 95-108.
[12] Shooshtari A., Razavi S., 2015, Large amplitude free vibration of symmetrically laminated magneto-electro-elastic rectangular plates on Pasternak type foundation, *Mechanics Research Communications* **69**: 103-113.
[13] Mohammadimehr M., Rostami R., Arefi M., 2016, Electro-elastic analysis of a sandwich thick plate considering FG core and composite piezoelectric layers on Pasternak foundation using TSDT, *Steel and Composite Structures* **20**: 513-543.
[14] Ansari R., Gholami R., Rouhi H., 2015, Size-dependent nonlinear forced vibration analysis of magneto-electro-thermo-elastic Timoshenko Nano beams based upon the nonlocal elasticity theory, *Composite Structures* **126**: 216-226.
[15] Xin L., Hu Z., 2015, Free vibration of layered magneto-electro-elastic beams by SS-DSC approach, *Composite Structures* **125**: 96-103.
[16] Xin L., Hu Z., 2015, Free vibration of simply supported and multilayered magneto-electro-elastic plates, *Composite Structures* **121**: 344-350.
[17] Mohammadimehr M., Monajemi A.A., Moradi M., 2015, Vibration analysis of viscoelastic tapered micro-rod based on strain gradient theory resting on visco-Pasternak foundation using DQM, *Journal of Mechanical Science and Technology* **29** (6): 2297-2305.
[18] Rahmati A.H., Mohammadimehr M., 2014, Vibration analysis of non-uniform and non-homogeneous boron nitride nanorods embedded in an elastic medium under combined loadings using DQM, *Physica B: Condensed Matter* **440**: 88-98.
[19] Ke L.L., Wang Y.S., 2014, Free vibration of size-dependent magneto-electro-elastic Nano beams based on the nonlocal theory, *Phisyca E* **63**: 52-61.
[20] Wang Y., Xu R., Ding H., 2011, Axisymmetric bending of functionally graded circular magneto-electro-elastic plates, *European Journal of Mechanics-A/Solid* **30**: 999-1011.
[21] Rao M.N., Schmidt R., Schröder K.U., 2015, Geometrically nonlinear static FE-simulation of multilayered magneto-electro-elastic, *Composite Structures* **127**: 120-131.
[22] Mohammadimehr M., Rousta Navi B., Ghorbanpour Arani A., 2015, Free vibration of viscoelastic double-bonded polymeric nanocomposite plates reinforced by FG-SWCNTs using MSGT, sinusoidal shear deformation theory and meshless method, *Composite Structures* **131**: 654-671.
[23] Mohammadimehr M., Rousta Navi B., Ghorbanpour Arani A., 2016, Modified strain gradient Reddy rectangular plate model for biaxial buckling and bending analysis of double-coupled piezoelectric polymeric nanocomposite reinforced by FG-SWNT, *Composite Part B: Engineering* **87**: 132-148.
[24] Kattimani S.C., Ray M.C., 2015, Control of geometrically nonlinear vibrations of functionally graded magneto-electro-elastic plates, *International Journal of Mechanical Sciences* **99**: 154-167.
[25] Liu Y., Han Q., Li C., Liu X., Wu B., 2015, Guided wave propagation and mode differentiation in the layered magneto-electro-elastic hollow cylinder, *Composite Structures* **132**: 558-566.
[26] Sedighi H. M., Farjam N., 2016, A modified model for dynamic instability of CNT based actuators by considering rippling deformation, tip-charge concentration and Casimir attraction, *Microsystem Technologies* **23**: 2175-2191.
[27] Zare J., 2015, Pull-in behavior analysis of vibrating functionally graded micro-cantilevers under suddenly DC voltage, *Journal of Applied and Computational Mechanics* **1**(1): 17-25.
[28] Sedighi H. M., 2014, The influence of small scale on the pull-in behavior of nonlocal nano bridges considering surface effect, Casimir and van der Waals attractions, *International Journal of Applied Mechanics* **6**(3): 1450030.
[29] Fleck N. A., Hutchinson J. W., 1993, Phenomenological theory for strain gradient effects in plasticity, *Journal of the Mechanics and Physics of Solids* **41**(12): 1825-1857.
[30] Fleck N. A., Hutchinson J. W., 1997, Strain gradient plasticity, *Advances in Applied Mechanics* **33**: 296-358.

[31] Fleck N. A., Hutchinson J. W., 2001, A reformulation of strain gradient plasticity, *Journal of the Mechanics and Physics of Solids* **49**(10): 2245- 2271.
[32] Lam D.D.C., Yang F., Chong A.C.M., Wang J., Tong P., 2003, Experiments and theory in strain gradient elasticity, *Journal of the Mechanics and Physics Solids* **51**: 1477-1508.
[33] Akgöz B., Civalek Ö., 2013, A size-dependent shear deformation beam model based on the strain gradient elasticity theory, *International Journal of Engineering Science* **70**: 1-14.
[34] Mohammadimehr M., Salemi M., Rousta Navi B., 2016, Bending, buckling, and free vibration analysis of MSGT microcomposite Reddy plate reinforced by FG-SWCNTs with temperature- dependent material properties under hydro-thermo-mechanical loadings using DQM, *Composite Structures* **138**: 361-380.
[35] Gurtin M., Ian Murdoch A., 1975, A continuum theory of elastic material surfaces, *Archive for Rational Mechanics and Analysis* **57**: 291-323.
[36] Gurtin M., Ian Murdoch A., 1987, Surface stress in solids, *International Journal of Solids and Structures* **14**: 431-440.
[37] Mohammadimehr M., Rousta Navi B., Ghorbanpour Arani A., 2015, Surface stress effect on the nonlocal biaxial buckling and bending analysis of polymeric piezoelectric Nano plate reinforced by CNT using Eshelby-Mori-Tanaka approach, *Journal of Solid Mechanics* **7**(2): 173-190.
[38] Karimi M., Shokrani M. H., Shahidi A. R., 2015, Size-dependent free vibration analysis of rectangular nanoplates with the consideration of surface effects using finite difference method, *Journal of Applied and Computational Mechanics* **1**(3): 122-133.
[39] Ghorbanpour Arani A., Kolahchi R., Mosayebi M., Jamali M., 2016, Pulsating fluid induced dynamic instability of visco-double-walled carbon nano-tubes based on sinusoidal strain gradient theory using DQM and Bolotin method, *International Journal of Mechanics and Materials in Design* **12**(1): 17-38.
[40] Ansari R., Gholami R., Sahmani S., 2011, Free vibration analysis of size-dependent functionally graded microbeams based on the strain gradient Timoshenko beam theory, *Composite Structures* **94** : 221-228.
[41] Şimşek M., Kocatürk T., Akbaş Ş.D., 2013, Static bending of a functionally graded microscale Timoshenko beam based on the modified couple stress theory, *Composite Structures* **95**: 740-747.
[42] Li Y.S., Feng W.J., Cai Z.Y., 2014, Bending and free vibration of functionally graded piezoelectric beam based on modified strain gradient theory, *Composite Structures* **115**: 41-50.
[43] Ghorbanpour Arani A., Abdollahian M., Kolahchi R., 2015, Nonlinear vibration of a Nano beam elastically bonded with a piezoelectric Nano beam via strain gradient theory, *International Journal of Mechanical Sciences* **100**: 32-40.
[44] Ansari R., Mohammadi V., Faghih Shojaei M., Gholami R., Rouhi H., 2013, Nonlinear vibration analysis of Timoshenko Nano beams based on surface stress elasticity theory, *European Journal of Mechanics-A/Solid* **45** :143-152.
[45] Ke L.L., Wang Y.S., Wang Z.D., 2012, Nonlinear vibration of the piezoelectric Nano beams based on the nonlocal theory, *Composite Structures* **94**: 2038-2047.
[46] Şimşek M., 2011, Nonlocal effects in the forced vibration of an elastically connected double-carbon nanotube system under a moving nanoparticle, *Computational Materials Science* **50**: 2112-2123.
[47] Ghorbanpour Arani A., Mortazavi S.A., Kolahchi R., Ghorbanpour Arani A.H., 2015, Vibration response of an elastically connected double-Smart Nano beam-system based nano-electro-mechanical sensor, *Journal of Solid Mechanics* **7**: 121-130.
[48] Ghorbanpour Arani A., Atabakhshian V., Loghman A., Shajari A.R., Amir S., 2012, Nonlinear vibration of embedded SWBNNTs based on nonlocal Timoshenko beam theory using DQ method, *Phisyca B* **407**: 2549-2555.
[49] Murmu T., Pradhan S.C., 2009, Buckling analysis of a single-walled carbon nanotube embedded in an elastic medium based on nonlocal elasticity and Timoshenko beam theory and using DQM, *Phisyca E* **41**: 1232-1239.
[50] Civalek O., 2006, Harmonic differential quadrature-finite differences coupled approaches for geometrically nonlinear static and dynamic analysis of rectangular plates on elastic foundation, *Journal of Sound and Vibrations* **294**: 966-980.
[51] Akgoz B., Civalek O., 2011, Strain gradient elasticity and modified couple stress models for buckling analysis of axially loaded micro-scaled beams, *International Journal of Engineering Science* **49**: 1268-1280.
[52] Zhang B., He Y., Liu D., Gan Z., Shen L., 2014, Non - classical Timoshenko beam element based on the strain gradient elasticity theory, *Finite Element in Analysis and Design* **79**: 22-39.
[53] Ansari R., Gholami R., Darabi M.A., 2012, A non-linear Timoshenko beam formulation based on strain gradient theory, *Journal of Mechanics of Materials and Structures* **7**: 195-211.
[54] Ghorbanpour Arani A., Kolahchi R., Zarei M.Sh., 2015, Visco-surface-nonlocal piezo-elasticity effects on nonlinear dynamic stability of graphene sheets integrated with ZnO sensors and actuators using refined zigzag theory, *Composite Structures* **132**: 506-526.